A portable AI-powered rotifer tracking system for in-situ water quality assessment

Yunping Zhang, Yunfei Tian, Yuxing Li, and Edmund Y. Lam

Department of Electrical and Electronic Engineering, The University of Hong Kong, Pokfulam, Hong Kong SAR, China

ABSTRACT

Conventional optical microscopes face limitations in detecting certain water pollutants, such as transparent microplastics. Rotifers, microscopic freshwater organisms, are effective bio-indicators for assessing aquatic health due to their sensitivity to environmental changes. However, traditional rotifer-based water quality assessments are hindered by complex sample preparation, inaccuracies from sample transportation, and the use of bulky optical systems that require specialized expertise. To address these challenges, we present a low-cost, portable, AI-powered rotifer tracking microscope for on-site water quality assessment. This system integrates a 3D-printed open-source microscope with custom AI algorithms on a Raspberry Pi, enabling automated rotifer tracking and analysis without the need for sample transportation or specialized skills. Its compact, user-friendly, and cost-efficient design enhances accessibility for resource-limited areas. Validation with samples polluted by microplastics demonstrated the system's ability to detect changes in the behavioral dynamics of rotifers, proving its reliability for real-time aquatic health monitoring. This innovative system offers a practical, scalable solution for water quality management in diverse settings.

Keywords: water quality assessment, 3D-printed microscope, portable system, in-situ analysis, real-time assessment

1. INTRODUCTION

Real-time water quality assessment is critical for ensuring the safety and sustainability of aquatic ecosystems. In-situ monitoring plays a vital role in achieving this goal by enabling direct, on-site evaluation of water conditions.[1] However, many pollutants, such as nanoplastics (NPs) and microplastics (MPs), are challenging to detect using conventional microscopy without fluorescence staining due to their small size and transparency.[2,3] These materials often require advanced imaging techniques or chemical modifications to become visible under traditional optical systems, which increases the complexity and cost of monitoring. Recent works have demonstrated innovative approaches to address these challenges, including the use of multi-sensor information,[4–6] machine learning algorithms,[7] and alternative imaging methodologies for indirect detection.[8,9] This growing body of research highlights the importance of developing indirect detection methods to enable real-time, in-situ monitoring of these pollutants. Among these, the indirect approaches based on biological indicators offer several advantages, including high sensitivity to environmental changes, ease of observation, and ecological relevance. Rotifers, as bio-indicators, are valued for their quick response to changes in water chemistry, temperature, and pollution, serving as early warnings of environmental degradation.[9,10] Due to their rapid responsiveness and widespread distribution, portable systems plays a crucial role in tracking rotifer activity for assessing and monitoring water quality directly in the field, minimizing issues associated with the transition time from the sampling site to laboratory conditions.

3D printing has emerged as a powerful and accessible tool for designing and developing portable devices for scientific research. Its flexibility, reproducibility, and low-cost production using standard components and plastic parts make it an ideal choice for creating custom scientific instruments.[11] This advancement has given rise to numerous open-source science hardware projects, enabling researchers and science enthusiasts to use, iterate, and adapt existing designs for a variety of applications.[12,13] Among these, the OpenFlexure Microscope

Send correspondence to Edmund Lam: elam@eee.hku.hk

Multimodal Sensing and Artificial Intelligence for Sustainable Future, edited by Francesco Soldovieri, Pascal Picart, Vittorio Bianco, Claas Falldorf, Proc. of SPIE Vol. 13570, 135700S
2025 Published by SPIE · 0277-786X · doi: 10.1117/12.3062375

(OFM)[14] stands out as a portable microscopy platform that combines precise mechanical sample manipulation with a lightweight and compact design. The OFM has been successfully utilized in a wide range of applications, demonstrating its versatility and reliability as a tool for field-based scientific investigations.[15]

In this study, we develop a portable, AI-powered microscope system specifically designed for in-situ rotifer-based water quality assessment. By integrating a 3D-printed open-source microscope with AI-assisted tracking algorithms, the system enables real-time monitoring and analysis of rotifer behavior directly in the field. The hardware combines the OFM[14] platform with Raspberry Pi camera modules, while the software employs lightweight YOLOv8-based algorithms for real-time detection and tracking of rotifers. Behavioral metrics such as trace length, net displacement, mean speed, mean turning angle, and efficiency ratio are extracted to quantitatively assess rotifer movement and responses to environmental contaminants. We validate the system through experiments with water samples contaminated by nanoparticles (NPs) and microplastics (MPs), which allows us to distinguish between contaminated and uncontaminated samples and investigate the size-dependent effects of these contaminants on rotifer behavior. This portable, cost-effective system bridges the gap between advanced water quality assessment techniques and practical field applications, offering a scalable solution for real-time aquatic ecosystem monitoring.

2. METHOD

2.1 AI-powered water quality assessment system

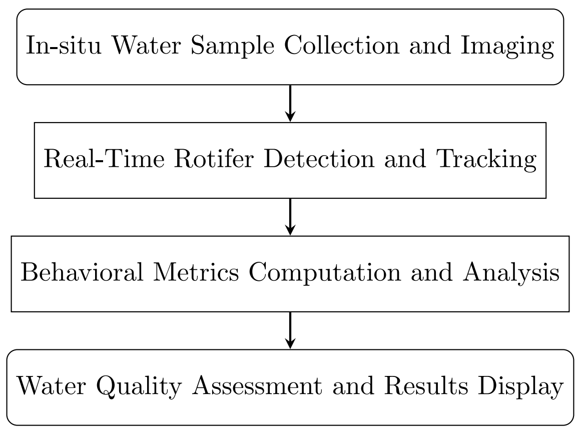

Figure 1. Flowchart of rotifer tracking system for in-situ water quality assessment.

The overall flowchart of our portable in-situ water quality assessment system is illustrated in Fig. 1. The process begins with collecting a water sample, which is then transferred using a pipette and placed on the sample stage of the portable microscope. Real-time imaging and tracking algorithms are executed directly on the Raspberry Pi via its command-line interface. The tracking algorithm used in this study is based on the YOLOv8 framework, which has shown exceptional performance in object detection tasks.[16,17] YOLOv8 is lightweight and energy-efficient, making it ideal for field deployment where power and computational resources are limited.[18] Once the model is trained, it enables real-time object detection even on devices with constrained processing capabilities, such as the Raspberry Pi.

2.2 Behavioral Metrics Extraction

After detecting and tracking the rotifers, their movement trajectories are extracted, and a series of behavioral metrics are calculated to quantitatively assess their activity. These metrics include trace length, net displacement, mean speed, mean turning angle, and efficiency ratio. The trace length L and net displacement D are two metrics that reflect the spatial extent of movement. The trace length represents the total distance traveled by a rotifer during the observation period, computed as the sum of the Euclidean distances between consecutive positions along its trajectory. In contrast, the net displacement measures the straight-line distance between the start and end points of the trajectory, ignoring the intermediate path. These are expressed mathematically as:

$$L = \sum_{i=1}^{N-1} \sqrt{(x_{i+1} - x_i)^2 + (y_{i+1} - y_i)^2}, \tag{1}$$

$$D = \sqrt{(x_N - x_1)^2 + (y_N - y_1)^2}. \tag{2}$$

Here (x_i, y_i) are the coordinates of the rotifer at time step i, and N is the total number of recorded positions. While trace length provides insight into the detailed motion activity, net displacement highlights the efficiency and directionality of the movement. The movement efficiency, also known as the efficiency ratio E, is characterized by the ratio of net displacement to trace length:

$$E = \frac{D}{L}. \tag{3}$$

An efficiency ratio of 1 indicates highly directed movement, while lower values suggest more exploratory motion. The mean speed $S = \frac{L}{T}$ is the average distance traveled per unit time, reflecting the overall pace of the rotifer's activity during the observation period T. It is defined as:

$$S = \frac{L}{T}. \tag{4}$$

The mean turning angle θ quantifies the angular changes in direction between consecutive trajectory segments, which is computed as:

$$\theta = \frac{1}{N-2} \sum_{i=2}^{N-1} \cos^{-1}\left(\frac{(x_{i+1} - x_i)(x_i - x_{i-1}) + (y_{i+1} - y_i)(y_i - y_{i-1})}{\sqrt{(x_{i+1} - x_i)^2 + (y_{i+1} - y_i)^2} \cdot \sqrt{(x_i - x_{i-1})^2 + (y_i - y_{i-1})^2}}\right). \tag{5}$$

These behavioral metrics collectively provide a comprehensive assessment of the rotifer's movement characteristics. They are indicative of the water's quality and potential contamination levels.

3. RESULTS

3.1 Tracking Rotifer Movements and Quantitative Analysis of Behavior

We first demonstrate the system's capability to track rotifer movements in real time using water samples contaminated with polystyrene (PS) nanoparticles (NPs) of varying sizes (30 nm, 500 nm, and 5 µm) and concentrations (0, 0.1, 1, 10, and 20 µg/ml). Rotifers were exposed to these conditions in 20 µg/ml culture tubes without food to mimic environmental exposure. Sampling and observations were conducted at 3h, 6h, 12h, and 24h, following standard protocols for acute toxicity studies.[19,20]

Fig. 2 illustrates the performance of our portable system in tracking rotifer movements. Ten randomly selected rotifer trajectories, extracted over a 3-minute observation period, are shown in Fig. 2(b). These trajectories demonstrate the system's ability to capture and represent the complex movement patterns of rotifers. The heatmap in Fig. 2(c) visualizes the movement intensity of rotifers across the observation area, weighted by their speed. To enhance visibility, the intensity values are scaled logarithmically. Brighter regions indicate areas where rotifers move with higher speeds or greater frequency, while darker regions represent lower-speed or less frequent movement. Black regions correspond to areas with no rotifer activity. Using the tracked trajectories, a series of behavioral metrics are calculated to quantitatively characterize rotifer movements as introduced in Section 2.2. These metrics are further analyzed in the following section to quantitatively assess the effects of pollutant exposure.

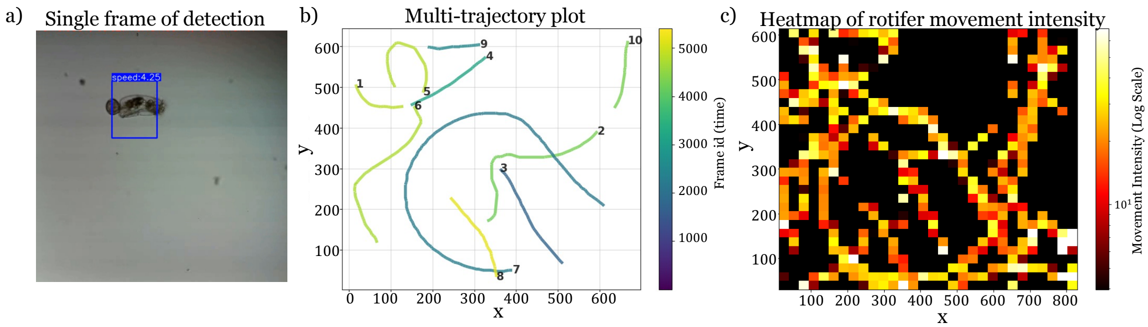

Figure 2. Demonstration of the proposed system in tracking rotifer movements. (a)Illustration of detected rotifer on a single frame by the system. (b)Ten randomly selected rotifer trajectories extracted over a 3-minute observation period, showcasing the system's ability to capture complex movement patterns. (c)Heatmap of rotifer movement intensity, weighted by speed and scaled logarithmically to enhance visibility. Brighter regions indicate areas of higher-speed or more frequent movement, while darker regions represent lower-speed or less frequent movement.

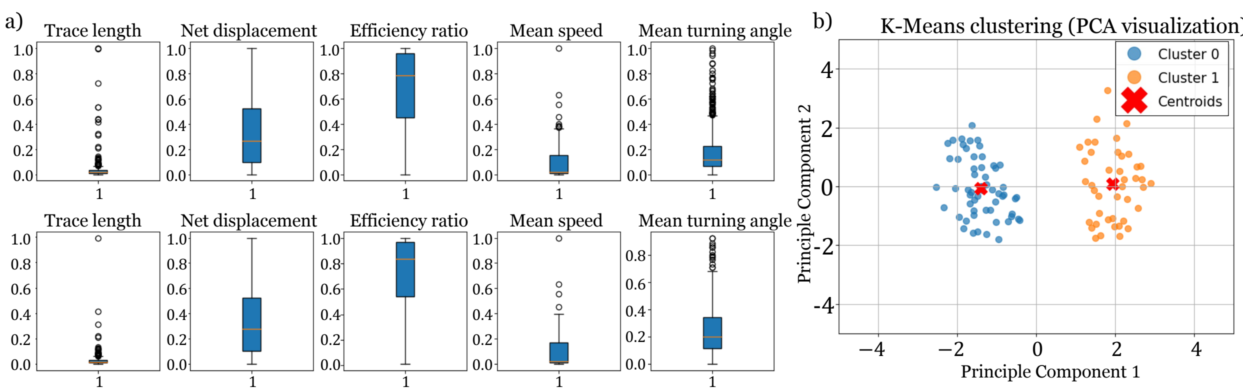

Figure 3. Unsupervised clustering of contaminated and uncontaminated samples using K-Means.(a) Box plots illustrating the process of outlier removal across different features. The upper row shows the data before outlier removal, and the bottom row displays the data after removal. The horizontal line within each box represents the median, while the boxes indicate the interquartile range (IQR). Whiskers extend to 1.5 times the IQR, with points outside this range identified and removed as outliers. (b) Visualization of K-Means clustering results after dimensionality reduction using PCA. Two clusters are represented in blue and orange, with red crosses indicating the centroids of each cluster.

3.2 Distinguishing Contaminated and Uncontaminated Samples

In this section, we demonstrate the application of our system in distinguishing contaminated and uncontaminated samples using behavioral metrics extracted from rotifer movements. Metrics introduced in Section 3.2.1 are analyzed to evaluate their effectiveness in differentiating between NPs-exposed experimental groups and control groups. To validate this approach, 100 randomly selected tracked trajectories from samples exposed to 30 nm NPs at a specific concentration of 10 µg/ml are compared to those from the control group after a 6-hour exposure period. Both unsupervised clustering (K-Means) and supervised classification (XGBoost) methods are employed to demonstrate the effectiveness of the selected behavioral metrics in distinguishing between contaminated and uncontaminated samples. These analyses highlight the potential of our system to utilize rotifer behavioral changes as reliable indicators for water quality assessment.

3.2.1 Unsupervised Clustering Analysis

For the unsupervised clustering analysis, K-Means clustering is employed with two clusters to distinguish between contaminated and uncontaminated samples. To account for the sensitivity of K-Means to feature scaling, the data is normalized using StandardScaler. Additionally, outliers are identified and removed to minimize their potential impact on clustering results. Outliers are defined as data points lying beyond 1.5 times the interquartile

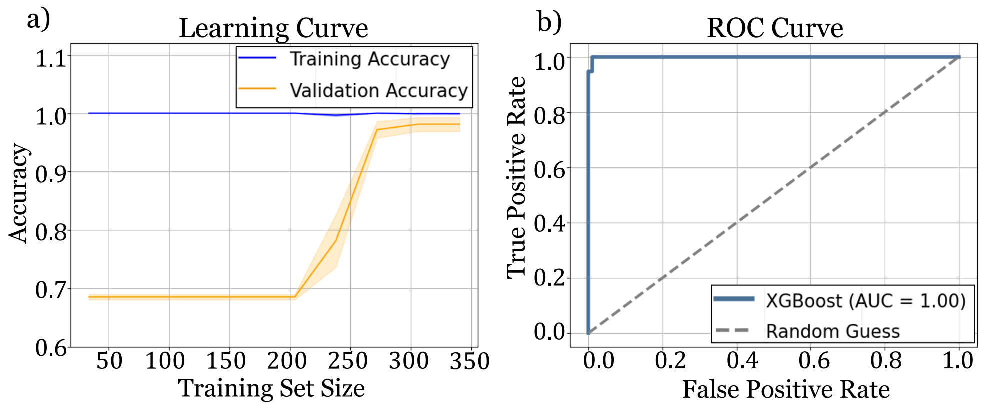

Figure 4. Performance evaluation of the supervised XGBoost classifier. (a) Learning curve plot. (b)ROC curve illustrating the classifier's performance to distinguish between the two classes across various decision thresholds. The random guess is represented by the diagonal line (AUC = 0.5).

range (IQR) above the third quartile (Q3) or below the first quartile (Q1). The effectiveness of this outlier removal process is shown in Fig. 3(a), where data points beyond the whiskers of the box plots are excluded as potential outliers. The quality of clustering is evaluated using the Silhouette Score, which is calculated to be 0.49. This metric assesses the separation between clusters, where a higher score (closer to 1) indicates better-defined clusters.[21] To facilitate visualization, Principal Component Analysis (PCA) is applied to reduce the dimensionality of the feature space to two dimensions. The resulting clustering is shown in Fig. 3(b), where the centroids are positioned near the center of their respective clusters. However, the proximity of the centroids in the reduced feature space suggests that the clusters are somewhat close, and the density of points within each cluster is uneven, contributing to the moderate Silhouette Score. This analysis demonstrates the potential of using behavioral metrics for unsupervised clustering, though further refinement may improve cluster separability.

3.2.2 Supervised Classification Analysis

Given the availability of labeled data, the supervised learning method can be utilized to train a machine learning model for predicting group labels (contaminated or uncontaminated) based on the extracted features. In our study, XGBoost is chosen for its ability to model complex decision boundaries effectively.[22] While deep learning methods could be considered for more complex classifications with larger datasets,[23] and zero-shot learning for entirely unseen samples,[7] we opted for a traditional machine learning algorithm (XGBoost) due to the specific characteristics of our dataset and computational resource constraints. This approach nonetheless yielded strong results, as demonstrated below. The dataset is split into a training set (80%) and a testing set (20%), and randomized search is applied to search for the best combination of hyperparameters by testing 50 randomly chosen configurations. The learning curve is shown in Fig. 4(a). As expected, the model achieves high accuracy on the training set, while the accuracy on the validation set gradually converges to 1.0 as the training size grows, demonstrating the model's ability to generalize well to unseen data.

In addition to accuracy, evaluation metrics such as precision, recall, and F1-score are calculated to provide a comprehensive assessment of the model's performance on the test set, which is reported in Table 1. To further evaluate the model's performance as a binary classifier, the receiver operating characteristic (ROC) curve is shown in Fig. 4(b), which plots the true positive rate (sensitivity) against the false positive rate across various classification thresholds. The ROC curve reaches a true positive rate of 1.0 with a negligible false positive rate, indicating near-perfect classification performance. The area under the curve (AUC) score is calculated to be 1.0, highlighting the model's exceptional ability to discriminate between the two classes.

Both the unsupervised clustering and supervised classification models demonstrate that the extracted metrics are key indicators of behavioral alterations caused by contamination. These findings confirm the system's potential as an effective tool for assessing water quality through rotifer behavior.

Table 1. Classification performance

	Precision	Recall	F1-Score
Control	0.98	1.00	0.99
Experimental	1.00	0.95	0.97

3.3 Investigation of Size-Dependent Impacts of NPs/MPs on Rotifer Behavior

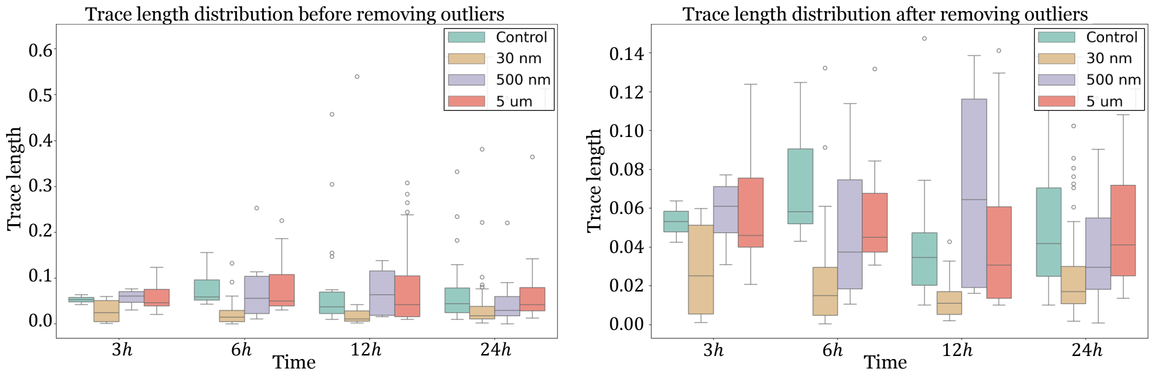

Figure 5. Trace length distributions before and after outlier removal. The initial distribution (left) shows significant variability in trace lengths, while the filtered distribution (right) demonstrates narrower and more consistent ranges across different conditions.

Our system's ability to assess water quality is further utilized to investigate rotifer behavior under NPs/MPs contamination of different sizes. Rotifer movement data under exposure to NPs/MPs with sizes of 30 nm, 500 nm, and 5 µm were collected using our system at 3h, 6h, 12h, and 24h. Due to the limited field-of-view, the collected traces may not capture the full movement of rotifers, leading to variability in trace lengths. As described in Section 3.2.1, an outlier removal process is applied to trace length data to minimize variability and ensure consistency in the analysis. This step allows us to focus on trajectories within a comparable range of lengths, providing reliable behavioral metric comparisons across experimental conditions. Fig. 5 illustrates the effectiveness of this pre-processing step. After applying outlier removal, the initial trace length distribution are condensed into narrower, more consistent ranges across all experimental conditions.

Following this, we calculate the behavioral metrics, including net displacement, mean speed, mean turning angle, and efficiency ratio, using the filtered data as shown in Fig. 6. The results demonstrate a size-dependent impact of NPs/MPs exposure on rotifer behavior. For instance, both the 30 nm and 500 nm groups exhibit a sharper decline in efficiency ratio over time compared to the 5 µm group, which remains closer to the control. Similarly, the speed reduction is more pronounced in the 30 nm and 500 nm groups, while the 5 µm group shows a relatively milder decline. These findings suggest that smaller particles (30 nm and 500 nm) reduce overall activity more significantly, likely due to their internal accumulation in rotifers, whereas larger particles (5 µm) have weaker effects, possibly due to their limited ability to accumulate internally and primarily causing external physical interference. The observed size-dependent toxicity of MPs/NPs on rotifer behavior aligns with prior studies on marine zooplankton.[19,20] However, our system achieves this using a simpler, more portable observation method that does not require fluorescence staining or complex optical systems, making it a more accessible and practical approach.

4. CONCLUSION

In this study, we developed a portable, AI-powered rotifer tracking system to enable in-situ water quality assessment. By leveraging advanced AI-based tracking algorithms, our system provides precise and automated behavioral metrics, including trace length, net displacement, mean speed, mean turning angle, and efficiency ratio. These metrics are used to assess rotifer responses to water contamination. Through a series of experiments,

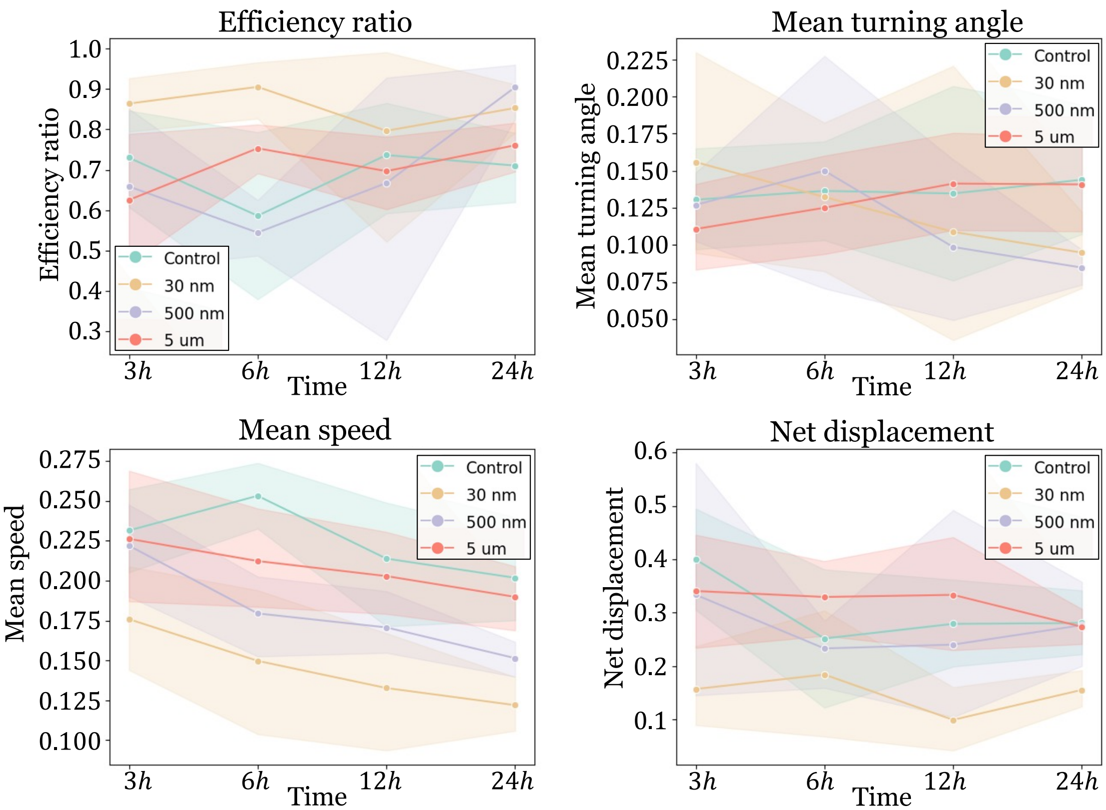

Figure 6. Behavioral metrics of rotifers under exposure to NPs/MPs of different sizes (30 nm, 500 nm, and 5 µm) over time (3h, 6h, 12h, and 24h).

we demonstrated the effectiveness of this system in tracking rotifer movements and performing quantitative behavioral analysis under various environmental conditions. Our system successfully distinguishes between contaminated and uncontaminated water samples and revealed size-dependent impacts of nanoplastics (NPs) and microplastics (MPs) on rotifer behavior. The system's simplicity, portability, and lack of dependence on fluorescence staining or complex optical setups make it a cost-effective solution for real-time, in-situ water quality monitoring. It offers a practical and efficient tool for assessing aquatic ecosystem health and advancing environmental conservation efforts.

5. ACKNOWLEDGMENT

The work is supported by the Research Grants Council of Hong Kong (RIF R7003-21).

REFERENCES

[1] Yan, T., Shen, S.-L., and Zhou, A., "Indices and models of surface water quality assessment: Review and perspectives," *Environmental Pollution* **308**, 119611 (2022).

[2] Zhu, Y., Li, Y., Huang, J., Zhang, Y., Ho, Y.-W., Fang, J. K.-H., and Lam, E. Y., "Advanced optical imaging technologies for microplastics identification: progress and challenges," *Advanced Photonics Research* **5**(11), 2400038 (2024).

[3] Xu, S., Wang, Q., Lao, J.-Y., Cao, Y., Hong, P., Chen, C., Lam, E. Y., Fang, J. K.-H., Lee, S., and Leung, K. M., "Typical tire additives in river water: Leaching, transformation, and environmental risk assessment," *Environmental Science & Technology* **58**(42), 18940–18949 (2024).

[4] Zhu, Y., Li, Y., Huang, J., and Lam, E. Y., "Smart polarization and spectroscopic holography for real-time microplastics identification," *Communications Engineering* **3**(1), 32 (2024).

[5] Huang, J., Zhu, Y., Li, Y., and Lam, E. Y., "Snapshot polarization-sensitive holography for detecting microplastics in turbid water," *ACS Photonics* **10**(12), 4483–4493 (2023).

[6] Zhu, Y., Zeng, T., Liu, K., Ren, Z., and Lam, E. Y., "Full scene underwater imaging with polarization and an untrained network," *Optics Express* **29**(25), 41865–41881 (2021).

[7] Zhu, Y., Lo, H. K. A., Yeung, C. H., and Lam, E. Y., "Microplastic pollution assessment with digital holography and zero-shot learning," *APL Photonics* **7**(7) (2022).

[8] Huang, L., Zhang, W., Zhou, W., Chen, L., Liu, G., and Shi, W., "Behaviour, a potential bioindicator for toxicity analysis of waterborne microplastics: A review," *TrAC Trends in Analytical Chemistry* **162**, 117044 (2023).

[9] Sarang, T. and Manoj, K., "Assessment of water quality of tapi river with reference to rotifera community," *J. Entomol. Zool. Stud* **9**, 2281–2284 (2021).

[10] Rico-Martínez, R., Arzate-Cárdenas, M. A., Robles-Vargas, D., Pérez-Legaspi, I. A., Jesús, A.-F., and Santos-Medrano, G. E., "Rotifers as models in toxicity screening of chemicals and environmental samples," in [*Invertebrates-Experimental Models in Toxicity Screening*], Larramendy, M. L. and Soloneski, S., eds., ch. 4, IntechOpen, Rijeka (2016).

[11] Diederich, B., Lachmann, R., Carlstedt, S., Marsikova, B., Wang, H., Uwurukundo, X., Mosig, A. S., and Heintzmann, R., "A versatile and customizable low-cost 3d-printed open standard for microscopic imaging," *Nature communications* **11**(1), 5979 (2020).

[12] Sharkey, J. P., Foo, D. C., Kabla, A., Baumberg, J. J., and Bowman, R. W., "A one-piece 3d printed flexure translation stage for open-source microscopy," *Review of Scientific Instruments* **87**(2) (2016).

[13] Danial, J. S., Lam, J. Y., Wu, Y., Woolley, M., Dimou, E., Cheetham, M. R., Emin, D., and Klenerman, D., "Constructing a cost-efficient, high-throughput and high-quality single-molecule localization microscope for super-resolution imaging," *Nature Protocols* **17**(11), 2570–2619 (2022).

[14] Collins, J. T., Knapper, J., Stirling, J., Mduda, J., Mkindi, C., Mayagaya, V., Mwakajinga, G. A., Nyakyi, P. T., Sanga, V. L., Carbery, D., et al., "Robotic microscopy for everyone: the openflexure microscope," *Biomedical Optics Express* **11**(5), 2447–2460 (2020).

[15] Knapper, J., Whiteford, F., Rosen, D., Wadsworth, W., Stirling, J., Mkindi, C., Mduda, J., Sanga, V. L., Nyakyi, P. T., Mboa Nkoudou, T. H., et al., "Developing the openflexure microscope towards medical use: technical and social challenges of developing globally accessible hardware for healthcare," *Philosophical Transactions A* **382**(2274), 20230257 (2024).

[16] Jiang, P., Ergu, D., Liu, F., Cai, Y., and Ma, B., "A review of yolo algorithm developments," *Procedia Computer Science* **199**, 1066–1073 (2022).

[17] Zhang, Y., Zhu, Y., and Lam, E. Y., "Holographic 3d particle reconstruction using a one-stage network," *Appl. Opt.* **61**, B111–B120 (Feb 2022).

[18] Sohan, M., Sai Ram, T., and Rami Reddy, C. V., "A review on yolov8 and its advancements," in [*International Conference on Data Intelligence and Cognitive Informatics*], 529–545, Springer (2024).

[19] Li, X., Lu, L., Ru, S., Eom, J., Wang, D., Wang, J., et al., "Nanoplastics induce more severe multigenerational life-history trait changes and metabolic responses in marine rotifer brachionus plicatilis: Comparison with microplastics," *Journal of Hazardous Materials* **449**, 131070 (2023).

[20] Jeong, C.-B., Won, E.-J., Kang, H.-M., Lee, M.-C., Hwang, D.-S., Hwang, U.-K., Zhou, B., Souissi, S., Lee, S.-J., and Lee, J.-S., "Microplastic size-dependent toxicity, oxidative stress induction, and p-jnk and p-p38 activation in the monogonont rotifer (brachionus koreanus)," *Environmental Science & Technology* **50**(16), 8849–8857 (2016).

[21] Rousseeuw, P. J., "Silhouettes: a graphical aid to the interpretation and validation of cluster analysis," *Journal of Computational and Applied Mathematics* **20**, 53–65 (1987).

[22] Chen, T. and Guestrin, C., "Xgboost: A scalable tree boosting system," in [*Proceedings of the 22nd acm sigkdd international conference on knowledge discovery and data mining*], 785–794 (2016).

[23] Zhu, Y., Hang Yeung, C., and Lam, E. Y., "Digital holographic imaging and classification of microplastics using deep transfer learning," *Applied Optics* **60**(4), A38–A47 (2021).